

# MASSM: An End-to-End Deep Learning Framework for Multi-Anatomy Statistical Shape Modeling Directly From Images

Janmesh Ukey, Tushar Kataria, and Shireen Y. Elhabian<sup>3</sup>

<sup>1</sup> Kahlert School of Computing, University of Utah

<sup>2</sup> Scientific Computing and Imaging Institute, University of Utah

<sup>3</sup> Corresponding author

{janmesh,tushar.kataria,shireen}@sci.utah.edu

**Abstract.** Statistical Shape Modeling (SSM) is an effective method for quantitatively analyzing anatomical variations within populations. However, its utility is limited by the need for manual segmentations of anatomies, a task that relies on the scarce expertise of medical professionals. Recent advances in deep learning have provided a promising approach that automatically generates statistical representations from unsegmented images. Once trained, these deep learning-based models eliminate the need for manual segmentation for new subjects. Nonetheless, most current methods still require manual pre-alignment of image volumes and specifying a bounding box around the target anatomy prior for inference, resulting in a partially manual inference process. Recent approaches facilitate anatomy localization but only estimate statistical representations at the population level. However, they cannot delineate anatomy directly in images and are limited to modeling a single anatomy. Here, we introduce MASSM, a novel end-to-end deep learning framework that simultaneously localizes multiple anatomies in an image, estimates population-level statistical representations, and delineates each anatomy. Our findings emphasize the crucial role of local correspondences, showcasing their indispensability in providing superior shape information for medical imaging tasks.

**Keywords:** Multi-Anatomy Networks · Deep Learning · Statistical Shape Modeling · Anatomy Detection

## 1 Introduction

Statistical Shape Modeling (SSM) is a powerful technique for quantifying and studying variations in anatomical forms. SSM has demonstrated its invaluable utility across a spectrum of biomedical and clinical applications, exemplified by studies and applications such as [12,4,16,9,3]. In shape analysis, a key technique entails using *landmarks* defined by their consistent anatomical correspondences across different subjects in a population. Traditionally, generating such correspondences has been a manual, time-consuming, and expertise-driven process,

posing challenges for 3D imaging and large datasets. Nonetheless, recent progress in shape modeling technology has significantly advanced the automation of *dense* landmark placement (correspondences or point distribution models, PDMs) on anatomical structures, streamlining the SSM process through optimization-based frameworks [10,8,11,21]. Even though such advancements reduce the need for expert manual identification of unique shape features, they do not entirely eliminate the necessity for expert-guided SSM workflows. SSM workflows still entail manual anatomy segmentation by professionals, shape registration, optimization of population-level shape representations, and extensive parameter tuning. Despite the technological progress, these steps remain time-intensive and costly, requiring considerable expert involvement.

Recently, deep learning has significantly improved SSM workflows, providing an automated approach to deriving statistical representations of anatomies directly from unsegmented images [7,6,1,2,19,13,17,23,24,18,14,5]. Once properly trained, these deep learning models eliminate the need for manual segmentation for new subjects, thereby streamlining the derivation of PDMs on new subjects during deployment. Nevertheless, these approaches continue to require image pre-processing, including anatomy extraction and rigid alignment—that is, cropping the images around the anatomy of interest and aligning them with a reference shape during both the training and inference phases. This prerequisite challenges the deployment of these methods as a fully automated alternative solution for conventional, optimization-based SSM methods. Recently, [20] has addressed the challenges of anatomy localization and rigid pose alignment. However, they primarily estimate population-level statistical representations of anatomies. Although this incorporation of shape priors regularizes the learning process, it simultaneously restricts the method’s utility in delineating anatomy within the image space. To the best of our knowledge, no existing method simultaneously provides population-level shape statistics and anatomy delineation. Moreover, existing approaches are designed to operate exclusively for a single anatomy, necessitating the training of a separate model for each specific anatomical structure. This requirement limits scalability, particularly for on-demand image-based diagnostics. Furthermore, this single-anatomy approach fails to leverage the shared characteristics inherent to anatomical structures, which could otherwise enhance the model’s accuracy and generalizability across different anatomies.

In this paper, we introduce MASSM, a multi-anatomy deep learning framework that simultaneously detects multiple anatomies within an image, estimates population-level statistical shape representation of each detected anatomy, and accurately delineates each anatomy within the image. Our method demonstrates comparable results to the models trained on single anatomy individually for world correspondences. Furthermore our local correspondences provide a better surface to surface estimate when compared to the fully supervised segmentation methods.

## 2 Methods

Given a dataset of  $N$  samples, we denote the 3D images as  $\{\mathbf{I}_n \in \mathbb{R}^{H \times W \times D}\}_{n=1}^N$ . MASSM generates 3D local and world correspondences for different anatomies present in  $\mathbf{I}_n$ . The architecture has three main networks: (1) anatomy detection in the volume, (2) 3D local correspondences prediction, and (3) 3D world correspondences prediction. The block diagram of the full framework is shown in Figure 1.

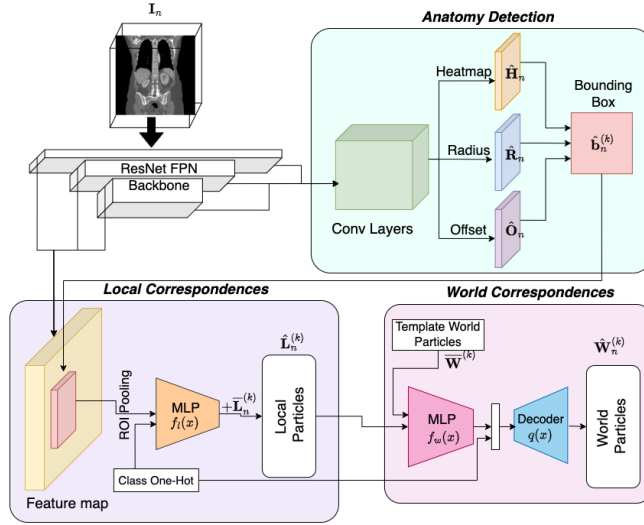


**Fig. 1. Multi-Anatomy Statistical Shape Model (MASSM).** Block diagram of the proposed end-to-end method to obtain statistical shape representation of multiple anatomies simultaneously. The proposed model has three networks; (a) *Anatomy Detection*, which extracts different anatomies of interest; (b) *Local Correspondences*, which predicts local particle correspondences and; (c) *Global Correspondences*, which predicts global correspondences.

### 2.1 Anatomy Detection

The detection block uses CenterNet [25] architecture with a 3D ResNet-101 FPN backbone. Let  $(cx_n^{(k)}, cy_n^{(k)}, cz_n^{(k)})$  be the ground truth center of anatomy of class  $k \in k = 1 \dots K$  in image  $\mathbf{I}_n$ , where  $K$  is the total number of anatomies. Let  $(rx_n^{(k)}, ry_n^{(k)}, rz_n^{(k)})$  be the radius from center that forms the bounding box over anatomy  $k$ . The detection model uses fusion of multi-resolution features to predict the center heatmap map  $\hat{\mathbf{H}}_n \in \mathbb{R}^{K \times \frac{H}{R} \times \frac{W}{R} \times \frac{D}{R}}$ , the radius map  $\hat{\mathbf{R}}_n \in \mathbb{R}^{3 \times \frac{H}{R} \times \frac{W}{R} \times \frac{D}{R}}$  and the offset map  $\hat{\mathbf{O}}_n \in \mathbb{R}^{3 \times \frac{H}{R} \times \frac{W}{R} \times \frac{D}{R}}$ , where  $R$  is the output stride. The center heatmap predicts the possible center of the anatomy, these however are predicted on strided output dimensions and do not correspond to real centers in the image, hence the offset map provides the offset from the

center in the heatmap to the real center. The radius map predicts the radius of the bounding box.

Using the predicted heatmap center  $(hx_n^{(k)}, hy_n^{(k)}, hz_n^{(k)})$  and predicted offset  $(ox_n^{(k)}, oy_n^{(k)}, oz_n^{(k)})$ , the true center of the anatomy is extracted using

$$\begin{aligned}\hat{cx}_n^{(k)} &= hx_n^{(k)} \times R + ox_n^{(k)} \\ \hat{cy}_n^{(k)} &= hy_n^{(k)} \times R + oy_n^{(k)} \\ \hat{cz}_n^{(k)} &= hz_n^{(k)} \times R + oz_n^{(k)}\end{aligned}$$

We also use the predicted heatmap centers  $(hx_n^{(k)}, hy_n^{(k)}, hz_n^{(k)})$  to extract the corresponding bounding box radii  $(r\hat{x}_n^{(k)}, r\hat{y}_n^{(k)}, r\hat{z}_n^{(k)})$  from the radius map. The object detection component is trained using focal loss for heatmap ( $L_h$ ) and the offset map ( $L_o$ ), and masked MSE loss for the radius map ( $L_r$ ).

$$\begin{aligned}\mathcal{L}_h &= \frac{1}{N} \sum \begin{cases} (1 - \hat{\mathbf{H}}_n)^\alpha \log(\hat{\mathbf{H}}_n), & \text{if } \mathbf{H}_n = 0 \\ (1 - \mathbf{H}_n)^\beta (\hat{\mathbf{H}}_n)^\alpha \log(1 - \hat{\mathbf{H}}_n), & \text{otherwise} \end{cases} \\ \mathcal{L}_r &= \frac{1}{N} \sum \|\hat{\mathbf{R}}_n - \mathbf{R}_n\|^2 \\ \mathcal{L}_o &= \frac{1}{N} \sum \frac{\|\hat{\mathbf{O}}_n - \mathbf{O}_n\|^2}{1 + \exp a \cdot (c - \|\hat{\mathbf{O}}_n - \mathbf{O}_n\|)}\end{aligned}$$

Here,  $(\alpha, \beta)$  and  $(a, c)$  are hyperparameters of  $L_h$  and  $L_o$  respectively. For all our experiments we set  $\alpha = 3$ ,  $\beta = 4$ ,  $a = 10$  and  $c = 0.2$ .

## 2.2 Local Correspondences

For shape analysis, we characterize shape as the residual information remaining after eliminating global alignment differences across samples within a given cohort. The Point Distribution Model (PDM) representing population-level statistical shape information after global alignment removal is termed as world correspondences. The PDM capturing this information in image space before eliminating global alignment is referred to as local correspondences. For  $k^{th}$  anatomy in the full 3D image  $\mathbf{I}_n$ , let  $(\hat{cx}_n^{(k)}, \hat{cy}_n^{(k)}, \hat{cz}_n^{(k)})$  and  $(r\hat{x}_n^{(k)}, r\hat{y}_n^{(k)}, r\hat{z}_n^{(k)})$  be the predicted center and radius of the bounding box  $\mathbf{b}_n^{(k)}$ , respectively. For each bounding box detection, the corresponding multi-resolution ROI features are extracted from the FPN backbone. ROI pooling then fuses these features into a single 1D vector. A one-hot vector corresponding to class  $k$  is appended to create a final feature vector for a single anatomy. This class-appended feature vector is given as input to an MLP layer ( $f_l(x)$ ) to predict the displacement for each local particle.

Let  $\mathbf{L}_n^{(k)}$  represent the local correspondences/particles for an anatomy  $k$  in an image  $\mathbf{I}_n$ . The set of corresponding PDMs is comprised of  $M$  3D correspondence points  $\mathbf{L}_n^{(k)} \in \mathbb{R}^{3M}$ , which are coordinates representing the population-level statistics in the image space. Let  $\bar{\mathbf{L}}^{(k)}$  represent the local correspondences of the template shape for anatomy  $k$ . The center of  $\bar{\mathbf{L}}^{(k)}$  is then aligned to the predicted center  $(\hat{c}x_n^{(k)}, \hat{c}y_n^{(k)}, \hat{c}z_n^{(k)})$ , resulting in  $\bar{\mathbf{L}}_n^{(k)}$ . The predicted local correspondences  $\hat{\mathbf{L}}_n^{(k)}$  will be defined by

$$\hat{\mathbf{L}}_n^{(k)} = \bar{\mathbf{L}}_n^{(k)} + d \tanh f_l(x)$$

where,  $d = 2 \cdot \max(\hat{r}x_n^{(k)}, \hat{r}y_n^{(k)}, \hat{r}z_n^{(k)})$ , gives the maximum dimension of the bounding box. This component of the framework optimizes a Focal Loss ( $L_l$ ) between the estimated and the ground truth local particles. Here,  $a, c$  are the hyperparameters of  $L_l$ , which are set to  $a = 10$  and  $c = 0.2$  for all experiments.

$$L_l = \frac{1}{N} \sum \frac{\|\hat{\mathbf{L}}_n - \mathbf{L}_n\|^2}{1 + \exp a \cdot (c - \|\hat{\mathbf{L}}_n - \mathbf{L}_n\|)}$$

### 2.3 World Correspondences

The world PDM consists of  $M$  world 3D correspondence points denoted by  $\mathbf{W}_n^{(k)}$  where  $\mathbf{W}_n^{(k)} \in \mathbb{R}^{3M}$ . These are essentially coordinates representing the population-level statistical shape information after removing global alignment differences across samples in the given cohort. For each anatomy detection, the corresponding predicted local particles  $\hat{\mathbf{L}}_n^{(k)}$  and the template world correspondences for anatomy  $k$  ( $\bar{\mathbf{W}}^{(k)}$ ) are given as input to a MLP layer ( $f_w(x)$ ).

The MLP layer projects them to a 32-dimension latent vector that is decoded via a Conditional VAE ( $q(x)$ ) to give the corresponding world particles  $\hat{\mathbf{W}}_n^{(k)}$ . This conditional VAE decoder has been pretrained to reconstruct the world particles.

$$\hat{\mathbf{W}}_n^{(k)} = q(f_w(\hat{\mathbf{L}}_n^{(k)}, \bar{\mathbf{W}}^{(k)}))$$

This component of the framework optimizes a Focal Loss ( $L_w$ ) between the estimated and the ground truth world particles.

$$L_w = \frac{1}{N} \sum \frac{\|\hat{\mathbf{W}}_n - \mathbf{W}_n\|^2}{1 + \exp a \cdot (c - \|\hat{\mathbf{W}}_n - \mathbf{W}_n\|)}$$

where  $a, c$  are the hyperparameters of  $L_w$ , which are set to  $a = 10$  and  $c = 0.2$  for all experiments.

## 2.4 End-to-End MASSM

Anatomy detection, local correspondences and world correspondences networks are connected as shown in Figure 1. The final loss used to train end-to-end MASSM is given by

$$L = \lambda_h L_h + \lambda_r L_r + \lambda_o L_o + \lambda_l L_l + \lambda_w L_w \quad (1)$$

where  $\lambda_h, \lambda_r, \lambda_o, \lambda_l, \lambda_w$  are hyperparameters.

## 3 Results and Discussion

**Training Details.** The model is trained in a phase-wise manner. The detection network is trained first with the initial hyperparameter values in equation (1) set to  $\lambda_h = 1$ ,  $\lambda_r = 0.01$  and  $\lambda_o = 1$ . After 20 epochs,  $\lambda_l$  is slowly increased with step size of 0.2 until it reaches the max value of 2 and  $\lambda_h$  is set to 40. After 40 epochs,  $\lambda_w$  is slowly increased with step size of 0.2 until it reaches the max value of 2.

Both local network and world network are initially trained using teacher forcing (conditioned on probability), and after 70 epochs only predicted values are used for training. Overall, we train the network for 300 epochs with an Adam [15] optimizer and an initial learning rate of 1e-4 with step learning rate decay of step size 20 and  $\gamma = 0.9$ .

**Datasets.** We train our model on the total segmentator dataset [22] that consists of 1188 CT scans. We select seven anatomies: heart ventricle left (HVL), heart ventricle right (HVR), heart atrium left (HAL), heart atrium right (HAR), lung upper lobe left (LULL), lung upper lobe right (LULR) and spleen (S). We divide the dataset into training and test sets and use ShapeWorks [8] to form the initial PDM with 1024 points from training set for each anatomy individually. In our experiments, the medoid shape is used as the template; where the medoid is selected by first computing the average segmentation and then selecting the training shape nearest to it.

### 3.1 Results

We compare our results with baseline DeepSSM [7] for both local and world correspondences prediction. DeepSSM.l refers to the model trained individually on full images to regress local particles. For world correspondences, we train two variations of DeepSSM [7], DeepSSM.w, and DeepSSMF.w. DeepSSMF.w uses full images to learn shape representation for each anatomy individually, whereas in DeepSSM.w, the images are first cropped and aligned as a pre-processing step, and then DeepSSM [7] is used for training shape representation for each anatomy.

For each organ, we evaluate the performance of each model by comparing the predicted world particles to their ground truths and computing the root mean squared error (RMSE) averaged over each dimension. We also reconstruct the

mesh from the predicted and ground truth particles and evaluate the surface-to-surface distance. Additionally for local correspondences, we train UNet as a baseline for each anatomy individually and use the predicted segmentations to reconstruct the mesh and compare the surface-to-surface distance. We provide the surface-to-surface distance visualization of reconstructed mesh for best cases in the test set for both local and world correspondences in Figure 4. More best and worst visualizations are available in supplementary Figure 5 and Figure 6.

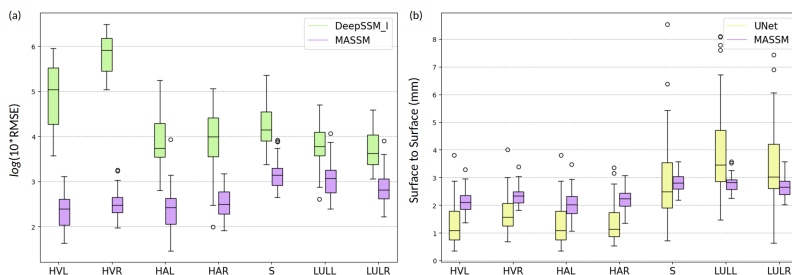


**Fig. 2. Performance on Local Particles** (a) RMSE (b) Surface-to-surface distance (mm) are reported for seven anatomies.

Figure 2 shows the box plots illustrating the RMSE and surface-to-surface distance for the reconstructed mesh on the test data. Our proposed end-to-end framework outperforms DeepSSM\_l on the RMSE metric by a large margin. Predicting local particles poses a considerable challenge, since it necessitates consideration of rigid transformations. Our method adeptly addresses this challenge through a modular approach. Initially, we pinpoint the center and solve for translation. Furthermore, the incorporation of a template provides a valuable prior over shape. Following alignment, the model efficiently tackles minor variations in a constrained setup, contributing to the observed performance boost. This modular methodology for predicting local particles is instrumental in enhancing overall performance. From Figure 2b, we can observe that MASSM obtains better performance for some anatomies than the UNet model when comparing surface-to-surface mesh distances. Our method demonstrates reduced sensitivity to outliers compared to segmentation techniques. Predicted segmentation from the UNet baseline frequently yields noisy labels, whereas correspondences adhere to a shape prior and are densely packed, resulting in more robust surface reconstructions. Figure 4 (a) reinforces this observation, as even in the best-case scenario for UNet, outliers are present, whereas MASSM consistently offers more uniform reconstructions. This trend persists in examples shown in Supplementary Figure 5.

The box plots for test data representing the RMSE and surface-to-surface distance for reconstructed mesh for world particles are shown in Figure 3. In contrast to DeepSSM\_w, our method exhibits inferior performance. It is worth noting that DeepSSM\_w was trained on cropped and aligned data specific to each anatomy, and therefore this baseline serves as the upper bound on performance.

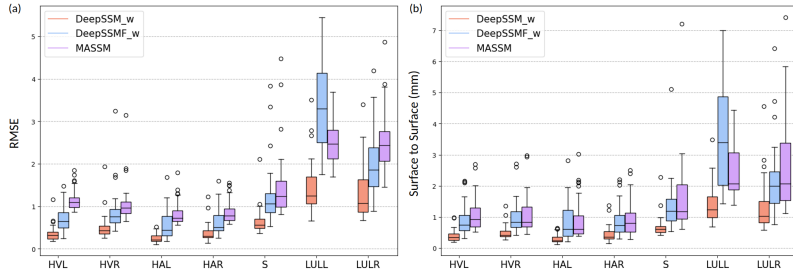


**Fig. 3. Performance on World Particles** (a) RMSE (b) Surface-to-surface distance (mm) are reported for seven anatomies.

Our proposed method does outperform DeepSSMF\_w on some anatomies, but does not consistently show the improvement. This outcome could be attributed to the limited variability in shape across the anatomies for the Total Segmentator. DeepSSM models tend to yield unsatisfactory results when confronted with shape variability [5]. This is demonstrated in Figure 3, for the left lung upper lobe, where DeepSSMF\_w performs worse, likely due to its higher variability compared to other anatomies. We attribute our method’s performance in higher variability to its reliance on local correspondences instead of image features. Once local particles are identified, the subsequent task involves aligning them to the template for world correspondence. This alignment step is comparatively easier to learn than extracting features directly corresponding to world shape information. In Figure 4 (b), the surface reconstruction heatmap for HVR is depicted. Notably, DeepSSM\_w demonstrates the most favorable performance, followed by MASSM and DeepSSMF\_w. This trend persists in additional examples shown in Supplementary Figure 6, where DeepSSM\_w consistently outperforms others, and MASSM and DeepSSMF\_w exhibit comparable or marginally different results from each other.

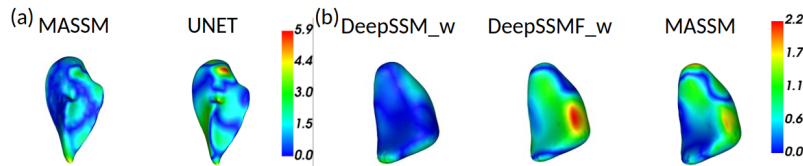


**Fig. 4. Surface-to-surface distance.** *Shape reconstruction error interpolated as a heatmap on ground truth reconstructed meshes.* (a) Local surface-to-surface with best case result on UNet for LULL. (b) World surface-to-surface with best case result on DeepSSM\_w for HVR.

## 4 Conclusion

MASSM is a end-to-end deep learning framework designed to extract population shape representations for multiple anatomies within an image simultaneously.



MASSM is the first model that predicts both local and world correspondences for multiple anatomies. This approach for deep learning-based shape modeling concurrently identifies the anatomy of interest while predicting its corresponding local and world statistical representations. Moreover, our method also eliminates the need for manual pre-processing of input images required by other shape modeling methods [7,6,1,2]. In comparison to the baseline DeepSSM models, our proposed model exhibits qualitative and quantitative performance that is comparable to the baselines for world correspondences. Additionally, it demonstrates superior results for local correspondences, even when comparing surface-to-surface distances with UNet. Our findings underscore the significance of local particles in providing superior shape information compared to segmentation, making them indispensable for medical imaging tasks.

## Acknowledgements

The National Institutes of Health supported this work under grant numbers NIBIB-U24EB029011 and NIAMS-R01AR076120. The content is solely the authors' responsibility and does not necessarily represent the official views of the National Institutes of Health.

## References

1. Adams, J., Bhalodia, R., Elhabian, S.: Uncertain-deepssm: From images to probabilistic shape models. In: International Workshop on Shape in Medical Imaging. pp. 57–72. Springer (2020)
2. Adams, J., Elhabian, S.: From images to probabilistic anatomical shapes: A deep variational bottleneck approach. arXiv preprint arXiv:2205.06862 (2022)
3. Atkins, P.R., Elhabian, S.Y., Agrawal, P., Harris, M.D., Whitaker, R.T., Weiss, J.A., Peters, C.L., Anderson, A.E.: Quantitative comparison of cortical bone thickness using correspondence-based shape modeling in patients with cam femoroacetabular impingement. *Journal of Orthopaedic Research* **35**(8), 1743–1753 (2017)
4. Atkins, P.R., Shin, Y., Agrawal, P., Elhabian, S.Y., Whitaker, R.T., Weiss, J.A., Aoki, S.K., Peters, C.L., Anderson, A.E.: Which two-dimensional radiographic measurements of cam femoroacetabular impingement best describe the three-dimensional shape of the proximal femur? *Clinical Orthopaedics and Related Research* **477**(1), 242 (2019)
5. Bhalodia, R., Elhabian, S., Adams, J., Tao, W., Kavan, L., Whitaker, R.: Deepssm: A blueprint for image-to-shape deep learning models. *Medical Image Analysis* **91**, 103034 (2024)
6. Bhalodia, R., Elhabian, S.Y., Kavan, L., Whitaker, R.T.: Deepssm: a deep learning framework for statistical shape modeling from raw images. In: International Workshop on Shape in Medical Imaging. pp. 244–257. Springer (2018)
7. Bhalodia, R., Goparaju, A., Sodergren, T., Morris, A., Kholmovski, E., Marrouche, N., Cates, J., Whitaker, R., Elhabian, S.: Deep learning for end-to-end atrial fibrillation recurrence estimation. In: 2018 Computing in Cardiology Conference (CinC). vol. 45, pp. 1–4. IEEE (2018)
8. Cates, J., Elhabian, S., Whitaker, R.: Shapeworks: particle-based shape correspondence and visualization software. In: Statistical Shape and Deformation Analysis, pp. 257–298. Elsevier (2017)
9. Datar, M., Cates, J., Fletcher, P.T., Gouttard, S., Gerig, G., Whitaker, R.: Particle based shape regression of open surfaces with applications to developmental neuroimaging. In: International Conference on Medical Image Computing and Computer-Assisted Intervention. pp. 167–174. Springer (2009)
10. Davies, R.H., Twining, C.J., Cootes, T.F., Waterton, J.C., Taylor, C.J.: A minimum description length approach to statistical shape modeling. *IEEE transactions on medical imaging* **21**(5), 525–537 (2002)
11. Durrleman, S., Prastawa, M., Charon, N., Korenberg, J.R., Joshi, S., Gerig, G., Trounevé, A.: Morphometry of anatomical shape complexes with dense deformations and sparse parameters. *NeuroImage* **101**, 35–49 (2014)
12. Harris, M.D., Datar, M., Whitaker, R.T., Jurrus, E.R., Peters, C.L., Anderson, A.E.: Statistical shape modeling of cam femoroacetabular impingement. *Journal of Orthopaedic Research* **31**(10), 1620–1626 (2013)
13. Huang, W., Bridge, C.P., Noble, J.A., Zisserman, A.: Temporal heartnet: towards human-level automatic analysis of fetal cardiac screening video. In: International Conference on Medical Image Computing and Computer-Assisted Intervention. pp. 341–349. Springer (2017)
14. Karanam, M.S.T., Kataria, T., Iyer, K., Elhabian, S.Y.: Adassm: Adversarial data augmentation in statistical shape models from images. In: International Workshop on Shape in Medical Imaging. pp. 90–104. Springer (2023)

15. Kingma, D.P., Ba, J.: Adam: A method for stochastic optimization. arXiv preprint arXiv:1412.6980 (2014)
16. Kozic, N., Weber, S., Büchler, P., Lutz, C., Reimers, N., Ballester, M.Á.G., Reyes, M.: Optimisation of orthopaedic implant design using statistical shape space analysis based on level sets. *Medical image analysis* **14**(3), 265–275 (2010)
17. Milletari, F., Rothberg, A., Jia, J., Sofka, M.: Integrating statistical prior knowledge into convolutional neural networks. In: *International Conference on Medical Image Computing and Computer-Assisted Intervention*. pp. 161–168. Springer (2017)
18. Raju, A., Miao, S., Jin, D., Lu, L., Huang, J., Harrison, A.P.: Deep implicit statistical shape models for 3d medical image delineation. In: *Proceedings of the AAAI Conference on Artificial Intelligence*. vol. 36, pp. 2135–2143 (2022)
19. Tao, W., Bhalodia, R., Elhabian, S.: Learning population-level shape statistics and anatomy segmentation from images: A joint deep learning model. arXiv preprint arXiv:2201.03481 (2022)
20. Ukey, J., Elhabian, S.: Localization-aware deep learning framework for statistical shape modeling directly from images. In: *Medical Imaging with Deep Learning* (2023)
21. Vicory, J., Pascal, L., Hernandez, P., Fishbaugh, J., Prieto, J., Mostapha, M., Huang, C., Shah, H., Hong, J., Liu, Z., et al.: Slicersalt: Shape analysis toolbox. In: *Shape in Medical Imaging: International Workshop, ShapeMI 2018, Held in Conjunction with MICCAI 2018, Granada, Spain, September 20, 2018, Proceedings*. pp. 65–72. Springer (2018)
22. Wasserthal, J., Breit, H.C., Meyer, M.T., Pradella, M., Hinck, D., Sauter, A.W., Heye, T., Boll, D.T., Cyriac, J., Yang, S., et al.: Totalsegmentator: Robust segmentation of 104 anatomic structures in ct images. *Radiology: Artificial Intelligence* **5**(5) (2023)
23. Xie, J., Dai, G., Zhu, F., Wong, E.K., Fang, Y.: Deepshape: Deep-learned shape descriptor for 3d shape retrieval. *IEEE transactions on pattern analysis and machine intelligence* **39**(7), 1335–1345 (2016)
24. Zheng, Y., Liu, D., Georgescu, B., Nguyen, H., Comaniciu, D.: 3d deep learning for efficient and robust landmark detection in volumetric data. In: *International conference on medical image computing and computer-assisted intervention*. pp. 565–572. Springer (2015)
25. Zhou, X., Wang, D., Krähenbühl, P.: Objects as points. arXiv preprint arXiv:1904.07850 (2019)

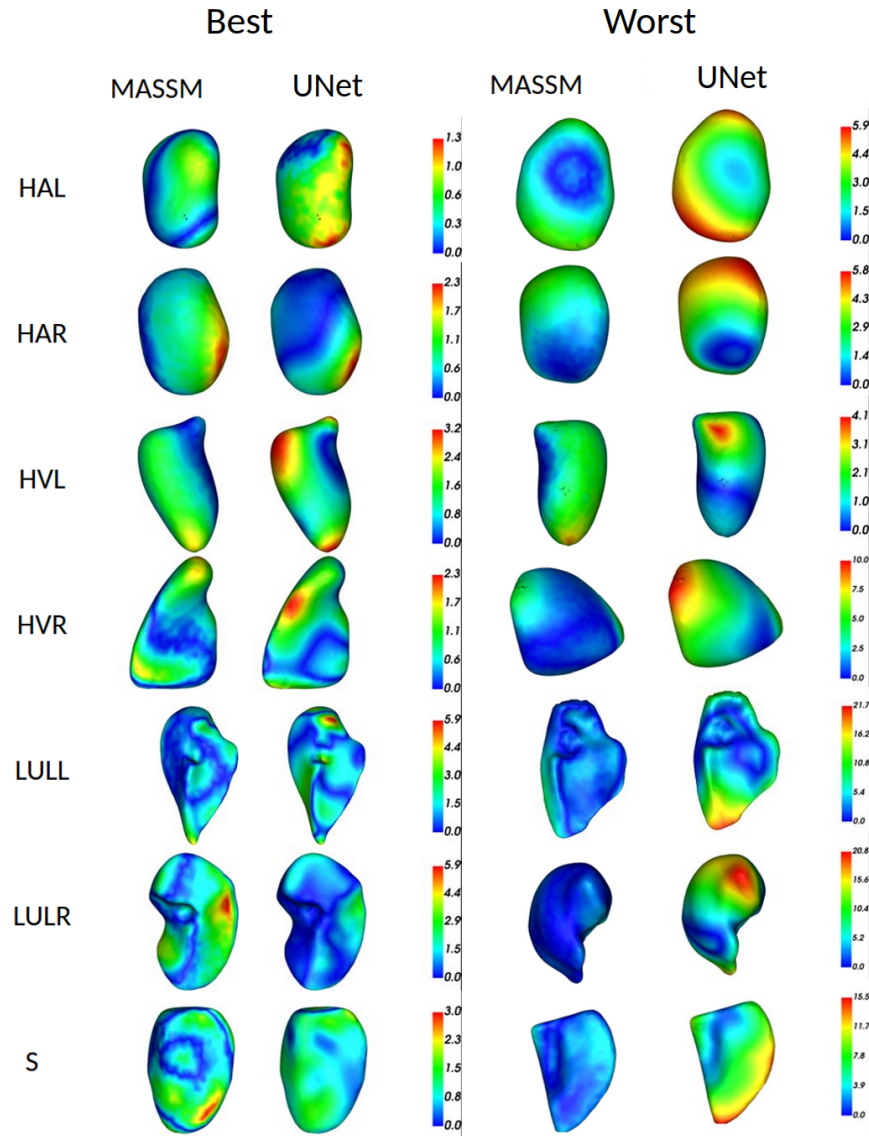


**Fig. 5. Surface to surface distance.** Best and worst case on shape reconstruction error for local correspondences, interpolated as a heatmap on ground truth reconstructed meshes, are reported for 7 anatomies.

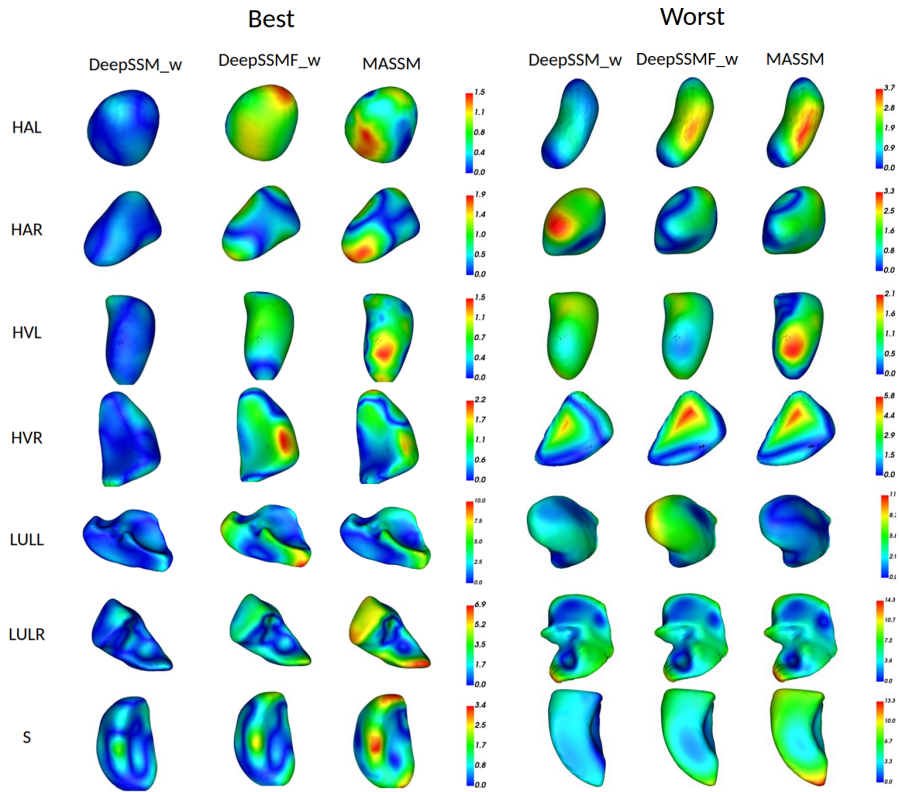


**Fig. 6. Surface to surface distance.** Best and worst case on shape reconstruction error for world correspondences, interpolated as a heatmap on ground truth reconstructed meshes, are reported for 7 anatomies.